A Risk-Adaptive TOPSIS Method for Electronic Decision Support in Vulnerable-Pedestrian Crossings

Zhuorui Li
School of Artificial Intelligence and Robotics, Hunan University of Technology and Business, Changsha 410205, Hunan, China
Corresponding author: 2431010049@stu.hutb.edu.cn

Abstract: Electronic decision support for vulnerable-pedestrian crossings requires heterogeneous factors, including crossing intention, individual vulnerability, traffic conditions, and roadside facilities, to be represented on a common scale. Fixed-weight multicriteria ranking cannot adapt its evaluation priorities to changes in scenario risk. This study proposes an electronic decision-support method that combines an intention-probability-driven risk model with risk-adaptive TOPSIS. The model integrates crossing-intention probability, vulnerability coefficient, traffic density, environmental adversity, and facility deficiency. A convex combination of baseline and scenario-dependent exponential weights produces a composite risk score, which continuously interpolates the TOPSIS criterion weights. The method ranks three intervention options and provides traceable intermediate results for human confirmation. In six reproducible simulated scenarios, the proposed method achieved a policy-level consistency rate of 100.0%, exceeding equal-weight and fixed-weight TOPSIS by 66.7 and 83.3 percentage points, respectively. Under ±10% weight perturbations, the mean preferred-option retention rate was 92.3%, and one risk evaluation and ranking required 31.8 ± 0.7 microseconds. The results show that the method adjusts evaluation priorities with scenario risk and generates intervention recommendations consistent with the predefined response level.

Keywords: intention probability; dynamic weighting; multicriteria ranking; scenario simulation; real-time computation

1 Introduction

Vulnerable pedestrians, including children, older adults, and people with mobility limitations, differ substantially in crossing speed, initiation time, and responses to road conditions. Roadside perception or intention-prediction modules can estimate crossing probability, but an electronic decision-support terminal must combine this probability with pedestrian attributes, traffic density, visibility, and facility status to generate actionable interventions. A fixed set of option-evaluation weights may produce the same ranking preference in both low- and high-risk situations. We therefore investigate intention-probability-driven risk quantification and risk-adaptive option ranking to integrate risk assessment, ranking, and result presentation into a coherent electronic decision-support chain.

Sharma et al. framed pose, trajectory, scene, and vehicle-motion information as a joint modeling problem and argued that prediction outputs should support subsequent vehicle decisions[1]. Ling and Ma reviewed visual features, contextual interactions, and evaluation protocols for open-road settings, identifying multisource information and temporal relations as central to open-scene modeling[2]. Landry and Akhloufi further summarized multimodal fusion, early prediction, and cross-scenario generalization[3]. Ma and Rong combined pedestrian appearance, motion, and road-context features[4], Chen et al. processed multisource inputs using a cross-modal Transformer and uncertainty-aware multitask learning[5], and Li et al. incorporated skeletal information to improve interpretability[6]. Wang and Lai, Xu et al., and Yang et al. advanced intention prediction through multimodal association, pedestrian-vehicle information modulation, and efficient feature fusion, respectively[7–9]. For temporal modeling, long-short observation-driven networks, progressive multimodal token fusion, and uncertainty-guided Transformer ensembles extract multiscale temporal cues, strengthen sequence representation, and explicitly address confidence variation[10–12]. Studies of ego-vehicle speed confounding, group-crossing intention, and multimodal context indicate that intention probabilities should be interpreted jointly with traffic state and road conditions[13–15]. In risk assessment, statistical conflict modeling, roadside-LiDAR intersection analysis, reviews of vulnerable-road-user trajectory prediction, and social-interaction modeling connect pedestrian behavior with road-safety requirements[16–20]. Multicriteria decision studies show that ANP-entropy TOPSIS can integrate subjective and objective information[21], while distributed TOPSIS retains the interpretability of ideal-solution distance ranking[22]. Research on artificial-intelligence decision support also emphasizes coordination among algorithmic output, human review, and result traceability[23, 24]. These studies provide foundations for intention prediction, risk assessment, and multicriteria ranking. However, electronic decision support still requires a unified risk scale for intention probability, vulnerability, and road conditions, together with evaluation priorities that change continuously with risk.

Based on this foundation, we formulate the problem as three consecutive operations: constructing a unified risk vector from intention probability and scene factors, mapping changes in risk to the criterion weights of candidate options, and producing a traceable option ranking. The method first combines baseline weights with scenario-dependent exponential weights to compute composite risk. It then interpolates between low- and high-risk endpoint weights to generate risk-adaptive TOPSIS weights. Unlike equal or fixed weighting, this chain retains predefined management preferences while propagating changes in high-valued risk factors to the intervention ranking.

The main contributions are as follows: (1) a unified risk model comprising crossing-intention probability, vulnerability coefficient, traffic density, environmental adversity, and facility deficiency; (2) a risk-score-driven method that continuously adjusts TOPSIS criterion weights and links option ranking to scenario risk; and (3) a traceable output process for baseline alerts, graded responses, and comprehensive interventions, evaluated using policy-level consistency, weight-perturbation retention, and runtime.

2 Materials and Methods

2.1 System Scope and Overall Architecture

The study considers an auxiliary decision module that can connect to roadside perception equipment and electronic warning terminals. At time t, the system receives pedestrian behavior, individual attributes, traffic state, environmental conditions, and crossing-facility information. An upstream module supplies a crossing-intention probability, the risk module calculates a composite score from 0 to 100, and the decision module ranks three options: baseline alert, graded response, and comprehensive intervention. The terminal reports the preferred option, alternative order, risk sources, criterion weights, and resource requirements while retaining a human-confirmation interface. Figure 1 summarizes the information chain.

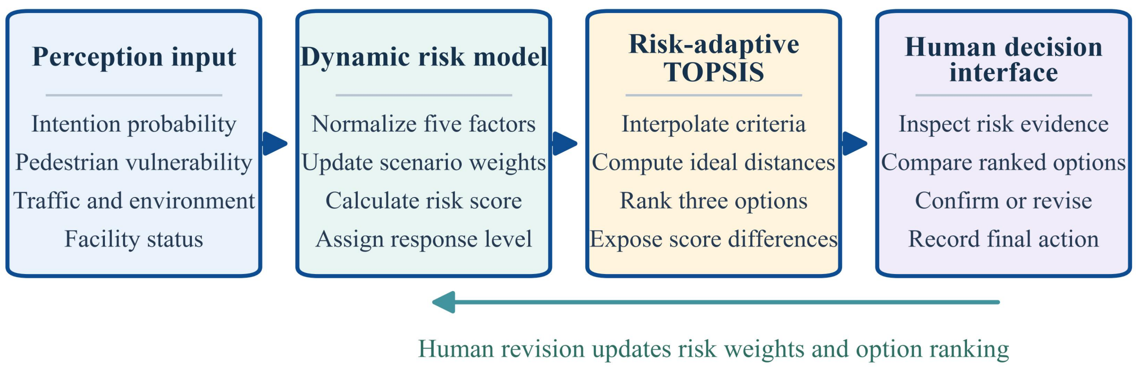

Figure 1 Overall architecture of electronic decision support for vulnerable-pedestrian crossings

2.2 Intention-Probability Input and Risk-Feature Vector

The interface separates the output of the upstream model from management variables. The intention probability may be provided by an LSTM, Transformer, skeletal model, or manually defined annotation rule, provided that it lies in [0,1]. Consequently, risk assessment does not depend on a specific prediction network and does not equate a probability output with prediction accuracy. The five-dimensional feature vector is defined as follows:

$$x_t = [p_t, v_t, \rho_t, e_t, f_t]^T \quad \textbf{(1)}$$

where x_t is the risk-feature vector at time t; p_t is the crossing-intention probability; v_t is the vulnerability coefficient; ρ_t is traffic density; e_t is environmental adversity; f_t is facility deficiency; and the superscript T denotes vector transposition.

For an upstream temporal window of length L, the interface can be expressed as the probability mapping:

$$p_t = \sigma(g_\theta(X_{t-L+1:t})) \quad \textbf{(2)}$$

where p_t is the crossing-intention probability at time t; σ is the sigmoid function; g_θ is a temporal prediction model parameterized by θ; $X_{t-L+1:t}$ is the observation sequence over the latest L time steps; and L is the window length.

The vulnerability coefficient is assigned according to categories such as children, older adults, and people with mobility limitations. Traffic density is normalized from flow or occupancy. Environmental adversity combines visibility, rainfall, and illumination, while facility deficiency describes the absence of signals, marked crossings, and separation facilities. All factors are restricted to [0,1], with larger values indicating higher risk. Figure 2 shows the feature settings used in the simulated scenarios.

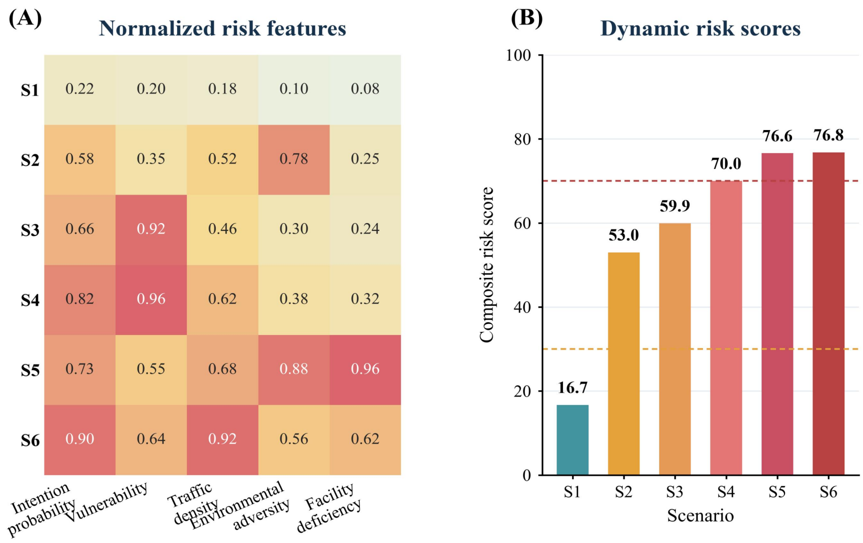

Figure 2 Risk-feature settings and dynamic risk scores for six scenarios: (A) normalized features; (B) risk-classification results

2.3 Dynamic Risk-Assessment Model

To allow risk weights to respond to scenario features while preserving reproducibility, a baseline weight w_j^0 is set and scenario-dependent exponential weights are generated from the current feature values. The scenario weight of factor j is defined as:

$$q_{j,t} = \frac{\exp(\beta x_{j,t})}{\sum_{l=1}^{5}\exp(\beta x_{l,t})} \quad \textbf{(3)}$$

where $q_{j,t}$ is the scenario-dependent exponential weight of factor j at time t; $x_{j,t}$ is the corresponding normalized feature; β is the weight-sensitivity coefficient; l is the summation index; and the number of factors is 5.

The scenario-dependent and baseline weights are combined convexly to prevent a single-frame feature from fully determining the weights:

$$w_{j,t}^{r} = (1-\lambda)w_{j}^{0} + \lambda q_{j,t} \quad \textbf{(4)}$$

where $w_{j,t}^{r}$ is the dynamic risk weight; w_j^0 is the baseline risk weight; $q_{j,t}$ is the scenario-dependent exponential weight; λ is the scenario-weight fusion coefficient; and $0 \leq \lambda \leq 1$.

The composite risk score weights the five features dynamically and maps the result to a 0-100 scale:

$$R_t = 100\sum_{j=1}^{5} w_{j,t}^{r} x_{j,t} \quad \textbf{(5)}$$

where R_t is the composite risk score at time t; $w_{j,t}^{r}$ is the dynamic weight of risk feature j; $x_{j,t}$ is risk feature j; and j is the factor index.

For an interpretable response hierarchy, the 0-100 risk scale is divided into 0-30, 31-70, and 71-100 intervals:

$$L(R_t) = \{\text{Low risk}, 0 \leq R_t \leq 30;\ \text{Medium risk}, 30 < R_t \leq 70;\ \text{High risk}, 70 < R_t \leq 100\} \quad \textbf{(6)}$$

where $L(R_t)$ is the risk-level function and R_t is the composite risk score. The three intervals correspond to low, medium, and high risk, respectively.

2.4 Risk-Adaptive TOPSIS Ranking

The candidate options are A, baseline alert; B, graded response; and C, comprehensive intervention. The criteria are safety benefit, response speed, coverage, cost efficiency, and implementation feasibility, all expressed as benefit criteria. Low-risk scenarios emphasize cost and feasibility, whereas high-risk scenarios emphasize safety and response. Decision weights are continuously interpolated between endpoint weight vectors:

$$\alpha_t = \left(\frac{R_t}{100}\right)^{\gamma}, w_{j,t}^{d} = (1-\alpha_t)w_j^{L} + \alpha_t w_j^{H} \quad \textbf{(7)}$$

where α_t is the risk-interpolation coefficient; R_t is the composite risk score; γ is the weight-change exponent; $w_{j,t}^{d}$ is the dynamic decision weight; and w_j^L and w_j^H are the low- and high-risk endpoint weights.

For m candidate options and n evaluation criteria, the original decision matrix is:

$$A = [a_{ij}]_{m\times n} \quad \textbf{(8)}$$

where A is the original decision matrix; a_{ij} is the attribute value of option i for criterion j; m is the number of candidate options; and n is the number of criteria.

Each criterion column is normalized using vector normalization:

$$v_{ij} = \frac{a_{ij}}{\sqrt{\sum_{k=1}^{m} a_{kj}^{2}}} \quad \textbf{(9)}$$

where v_{ij} is the normalized attribute value; a_{ij} is the original attribute value; k is the option index; and m is the number of options.

Multiplying the normalized matrix by the dynamic weights gives the weighted matrix:

$$y_{ij} = w_{j,t}^{d} v_{ij} \quad \textbf{(10)}$$

where y_{ij} is the weighted normalized value; $w_{j,t}^{d}$ is the dynamic decision weight of criterion j at time t; and v_{ij} is the normalized attribute value.

The positive and negative ideal solutions are the maximum and minimum weighted values for each criterion:

$$y_j^{+} = \max_i y_{ij}, y_j^{-} = \min_i y_{ij} \quad \textbf{(11)}$$

where y_j^+ is the positive ideal value of criterion j; y_j^- is the negative ideal value; y_{ij} is the weighted value of option i for criterion j; and i is the option index.

The Euclidean distances from option i to the positive and negative ideal solutions are:

$$D_i^{+} = \sqrt{\sum_{j=1}^{n}(y_{ij} - y_j^{+})^2}, D_i^{-} = \sqrt{\sum_{j=1}^{n}(y_{ij} - y_j^{-})^2} \quad \textbf{(12)}$$

where D_i^+ and D_i^- are the distances from option i to the positive and negative ideal solutions; n is the number of criteria; and j is the criterion index.

A larger relative closeness indicates that an option is nearer to the positive ideal solution:

$$C_i = \frac{D_i^{-}}{D_i^{+} + D_i^{-}} \quad \textbf{(13)}$$

where C_i is the relative closeness of option i; D_i^+ and D_i^- are the positive- and negative-ideal distances; and C_i lies in [0,1].

2.5 Decision Output and Human Confirmation

The system ranks the preferred and alternative options in descending order of C_i. It also presents the composite risk score, contributions of the five risk factors, criterion weights, and resource requirements. Low-risk scenarios may use advance notifications, audio alerts, or warning lights. Medium-risk scenarios add graded responses and personnel coordination. High-risk scenarios use traffic control, facility coordination, and on-site intervention. A manager may confirm, revise, or reject the preferred option, after which the revised input re-enters the ranking process.

This interaction assigns consistent computation to the model and road rules, available resources, and accountability boundaries to the human operator. When a risk score approaches a classification threshold, the system presents the two leading options and their closeness difference to avoid treating a small numerical difference as a categorical conclusion.

3 Experimental Design

3.1 Scenario Configuration and Model Parameters

Six scenarios were constructed from five risk variables and three intervention levels: signal-controlled daytime crossing, rainfall with low visibility, slow crossing by an older adult, sudden crossing by a child, nighttime crossing without signal facilities, and group crossing under dense traffic. Scenario variables were configured within [0,1] to examine the method's computational behavior under different risk combinations. They do not represent road-measurement statistics.

Table 1 Normalized configuration and risk calculation for the six scenarios

ID	Description	p_t	v_t	ρ_t	e_t	f_t	Score	Level
S1	Signal-controlled daytime	0.22	0.20	0.18	0.10	0.08	16.710	Low
S2	Rainfall and low visibility	0.58	0.35	0.52	0.78	0.25	52.994	Medium
S3	Slow crossing by an older adult	0.66	0.92	0.46	0.30	0.24	59.857	Medium
S4	Sudden crossing by a child	0.82	0.96	0.62	0.38	0.32	70.016	High
S5	Nighttime without signal facilities	0.73	0.55	0.68	0.88	0.96	76.563	High
S6	Group crossing under dense traffic	0.90	0.64	0.92	0.56	0.62	76.841	High

The baseline risk weights were (0.30, 0.20, 0.20, 0.15, 0.15), the scenario-fusion coefficient was $\lambda = 0.35$, and the exponential-weight sensitivity coefficient was $\beta = 2.5$. The low-risk decision endpoint was (0.20, 0.15, 0.10, 0.30, 0.25), and the high-risk endpoint was (0.50, 0.28, 0.17, 0.03, 0.02). The weight-change exponent was $\gamma = 1.5$. All parameters were fixed before the experiment, and the same configuration was used for every scenario.

3.2 Candidate-Option Attributes and Comparison Baselines

Three candidate options were defined according to intervention intensity and resource requirements. Baseline alert emphasizes response speed, cost efficiency, and implementation feasibility. Graded response balances safety benefit, response speed, and resource use. Comprehensive intervention emphasizes safety benefit and coverage but has lower cost efficiency and feasibility. Table 2 lists the normalized option attributes.

Table 2 Normalized decision matrix for the three candidate options

Candidate option	Safety benefit	Response speed	Coverage	Cost efficiency	Implementation feasibility
A Baseline alert	0.50	0.96	0.52	0.98	0.97
B Graded response	0.80	0.82	0.80	0.70	0.78

C Comprehensive intervention	0.99	0.68	0.98	0.34	0.46

The comparison methods were equal-weight TOPSIS and fixed-weight TOPSIS. Equal-weight TOPSIS assigned 0.20 to each of the five criteria, whereas fixed-weight TOPSIS always used the low-risk endpoint. The proposed method updated criterion weights from the risk score using Eq. (7). All three methods used the same decision matrix and normalization procedure and differed only in criterion weights.

3.3 Evaluation Metrics, Robustness, and Runtime

Policy-level consistency was used to determine whether the recommended option matched the predefined response level: baseline alert for low risk, graded response for medium risk, and comprehensive intervention for high risk. This metric evaluates decision logic rather than pedestrian-intention prediction accuracy. For S scenarios, consistency is defined as:

$$A = \frac{1}{S}\sum_{s=1}^{S} \mathrm{I}(r_s = r_s^*) \tag{14}$$

where A is the policy-level consistency rate; S is the number of scenarios; $I(.)$ is the indicator function; r_s is the recommended option in scenario s; and r_s^* is the predefined response level for the corresponding risk class.

For weight-sensitivity testing, each dynamic decision weight was independently multiplied by a random factor uniformly distributed over [0.9,1.1] and then renormalized to sum to 1. Each scenario was repeated 2,000 times using the fixed random seed 20260724. The preferred-option retention rate is defined as:

$$S_s = \frac{1}{N}\sum_{n=1}^{N} \mathrm{I}(\mathrm{argmax}_i C_i^{(n)} = \hat{\imath}_s) \tag{15}$$

where S_s is the preferred-option retention rate in scenario s; N is the number of perturbations; $C_i^{(n)}$ is the closeness of option i in perturbation n; and $\hat{\imath}_s$ is the preferred-option index under the unperturbed weights.

Runtime was measured using a single-threaded Python 3.12 script. Each run performed 5,000 consecutive risk calculations and option rankings. Ten runs were conducted, and the mean and sample standard deviation of the per-calculation runtime were reported.

4 Results

4.1 Dynamic Risk Scores and Classification

Figure 2B presents the risk scores. S1 scored 16.710 and was classified as low risk. S2 and S3 scored 52.994 and 59.857, respectively, and were classified as medium risk. S4 scored 70.016, marginally exceeding the high-risk threshold. S5 and S6 scored 76.563 and 76.841, respectively, and were classified as high risk. The dynamic risk model did not assign a level from the scenario name; the level resulted from the five features and their scenario-dependent weights.

The environmental-adversity value of S2 was 0.78, increasing the scenario weight of the environmental factor. The vulnerability coefficient of S3 was 0.92, increasing the contribution assigned to the older pedestrian. S5 combined high environmental adversity with substantial facility deficiency, while the intention probability and traffic density of S6 both exceeded 0.90. Under identical baseline weights, the exponential weighting reflected the dominant risk source of each scenario in the composite score.

4.2 Option Closeness and Recommendation Changes

Figure 3A shows the TOPSIS closeness of the three options under dynamic weighting. In S1, baseline alert achieved a closeness of 0.666, compared with 0.585 for graded response and 0.334 for comprehensive intervention. Graded response ranked first in S2 and S3, with closeness values of 0.591 and 0.593. Comprehensive intervention reached 0.641 and 0.643 in S5 and S6, exceeding 0.598 for graded response in both cases. The preferred option changed from A at low risk to B at medium risk and C at high risk, as intended by the continuous risk-dependent weighting.

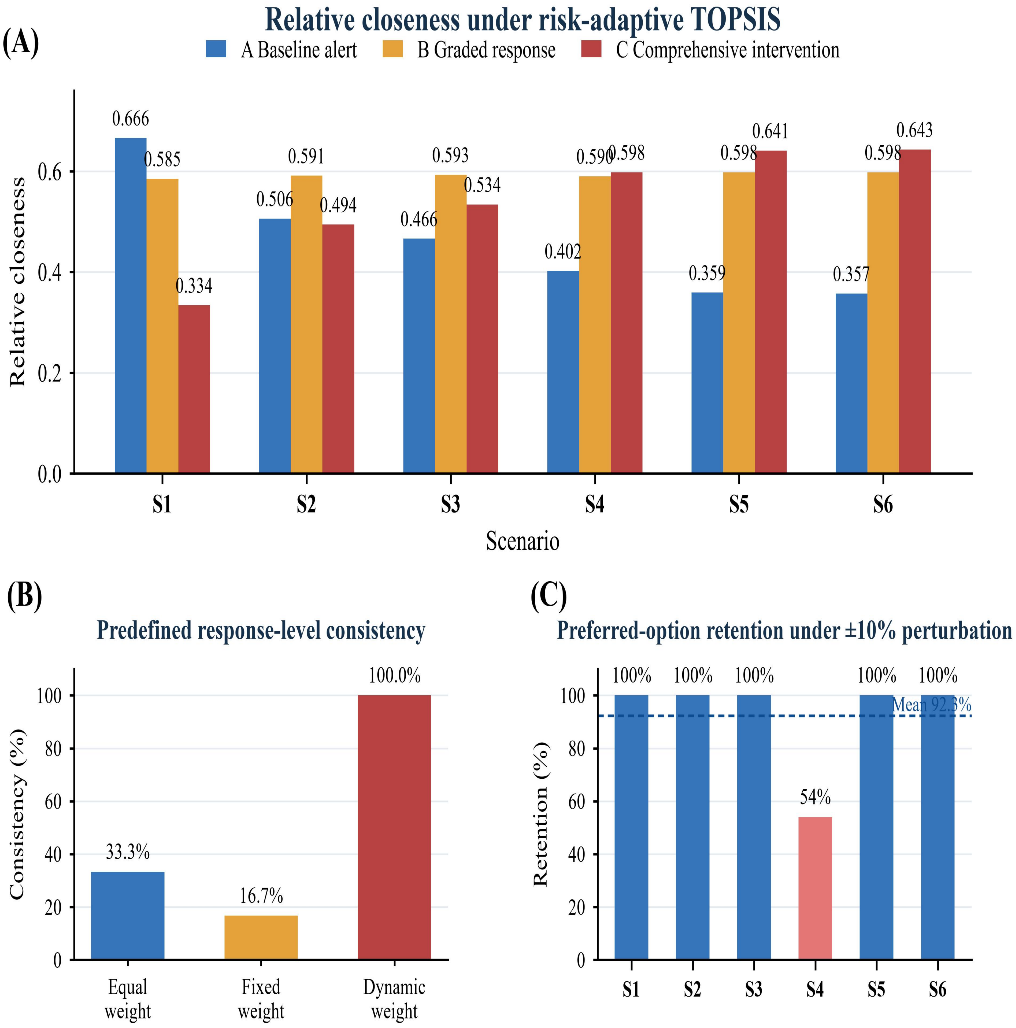

Figure 3 Option closeness, baseline consistency, and weight-perturbation stability: (A) TOPSIS closeness; (B) policy-level consistency; (C) preferred-option retention

Table 3 Scenario-level recommendations and weight-perturbation results for dynamic TOPSIS

ID	Risk level	Preferred option	Preferred closeness	Second closeness	Gap	Rate
S1	Low	A Baseline alert	0.666	0.585	0.082	100.0%
S2	Medium	B Graded response	0.591	0.506	0.085	100.0%
S3	Medium	B Graded response	0.593	0.534	0.059	100.0%
S4	High	C Comprehensive intervention	0.598	0.596	0.002	54.0%
S5	High	C Comprehensive intervention	0.641	0.598	0.043	100.0%
S6	High	C Comprehensive intervention	0.643	0.598	0.045	100.0%

In S4, the closeness values of comprehensive intervention and graded response were 0.598 and 0.596, respectively, a difference of only 0.002. The scenario score of 70.016 was near the medium-high risk boundary, and the preferred-option retention rate under ±10% weight perturbations was 54.0%. For such a case, the system presents both leading options and their difference so that the manager can determine whether available resources justify escalation to comprehensive intervention. The preferred option was retained in all perturbations for the other five scenarios.

4.3 Comparison, Robustness, and Runtime

Dynamic TOPSIS achieved 100.0% policy-level consistency, exceeding equal-weight TOPSIS at 33.3% by 66.7 percentage points and fixed-weight TOPSIS at 16.7% by 83.3 percentage points. Equal-weight TOPSIS preferred the same compromise option in four of the six scenarios, and fixed low-risk weights continued to favor low-cost options in high-risk scenarios. Dynamic TOPSIS matched the predefined response level in all six scenarios. The candidate-option attributes were unchanged; the ranking differences resulted solely from risk-driven changes in criterion weights.

The mean preferred-option retention rate across the six scenarios was 92.3%. S1, S2, S3, S5, and S6 retained their original preferred option in all 2,000 perturbations, whereas S4 yielded 54.0% because of its small closeness difference. One dynamic risk evaluation and TOPSIS ranking required 31.8 ± 0.7 microseconds, supporting its use as an immediate calculation module in a front-end interactive system.

5 Discussion

5.1 Risk Propagation and Option-Ranking Mechanism

The results correspond to the method structure at each stage. Risk features determine the scenario-dependent exponential weights, which are combined with baseline weights to produce a risk score. The risk score locates the criterion weights for safety, response, coverage, cost, and feasibility. These dynamic weights alter each option's distances to the positive and negative ideal solutions, and the resulting closeness ranking produces the recommendation. Every intermediate quantity can be displayed in a visual decision terminal, allowing a manager to trace a recommendation back to criterion weights and risk factors.

5.2 Fixed Parameters and Boundary-Scenario Handling

This computational order prevents retrospective method selection based on a particular result. Risk-classification thresholds, baseline weights, endpoint weights, the option-attribute matrix, and perturbation rules were fixed before the experiment. Scenario results were used only to determine whether the predefined method operated as specified. For boundary cases such as S4, the ranking is not presented as a categorical conclusion. Instead, decision support combines the closeness difference with human confirmation.

5.3 Computational Workflow of the Electronic Decision-Support Terminal

In deployment, roadside vision, LiDAR, or other perception modules can provide intention probabilities and traffic state, while individual attributes and facility status are entered through structured fields. After risk assessment and TOPSIS ranking, the terminal reports the risk score, dominant risk factors, option closeness, and preferred option. With three options and five criteria, one calculation required 31.8 ± 0.7 microseconds, allowing the terminal to update the ranking by frame or by event.

6 Conclusion

The proposed method maps crossing-intention probability, vulnerability coefficient, traffic density, environmental adversity, and facility deficiency to a common risk scale and continuously adjusts decision criteria using the resulting score. Across six reproducible simulated scenarios, risk-adaptive TOPSIS matched all predefined response levels and maintained a mean preferred-option retention rate of 92.3% under ±10% weight perturbations. Its 31.8 ± 0.7-microsecond runtime supports a traceable calculation chain from intention input and composite risk to option ranking and human-confirmed output.

Declarations

Conflict of Interest: [The author must confirm the conflict-of-interest declaration before submission.]

Funding: [The author must confirm the funding declaration before submission.]

Data and Code Availability: The six scenario configurations, calculation formulas, fixed random seed, and experimental scripts used in this study are available from the corresponding author upon reasonable request. The scenario data are reproducible configurations and do not represent road-measurement statistics.

Ethics Statement: This study did not involve identifiable personal information, human participants, or animals.

Author Contributions: Zhuorui Li contributed to study design, model development, experimental analysis, and manuscript preparation.

Generative AI Use Statement: Generative AI tools assisted with language editing, format checking, and portions of the figure code. The author reviewed and takes responsibility for the research question, algorithm definition, parameter settings, experimental interpretation, and final manuscript.

References

[1] Sharma N, Dhiman C, Indu S. Pedestrian Intention Prediction for Autonomous Vehicles: A Comprehensive Survey. *Neurocomputing*, 2022, 508: 120–152. https://doi.org/10.1016/j.neucom.2022.07.085.

[2] Ling Y, Ma Z. Pedestrian Crossing Intention Prediction in the Wild: A Survey. *CHAIN*, 2024, 1(4): 263–279. https://doi.org/10.23919/chain.2024.000008.

[3] Landry FG, Akhloufi MA. Predicting Pedestrian Crossing Intention in Autonomous Vehicles: A Review. *Neurocomputing*, 2025, 618: 129105. https://doi.org/10.1016/j.neucom.2024.129105.

[4] Ma J, Rong W. Pedestrian Crossing Intention Prediction Method Based on Multi-Feature Fusion. *World Electric Vehicle Journal*, 2022, 13(8): 158. https://doi.org/10.3390/wevj13080158.

[5] Chen X, Zhang S, Li J*, et al.*. Pedestrian Crossing Intention Prediction Based on Cross-Modal Transformer and Uncertainty-Aware Multi-Task Learning for Autonomous Driving. *IEEE Transactions on Intelligent Transportation Systems*, 2024, 25(9): 12538–12549. https://doi.org/10.1109/tits.2024.3386689.

[6] Li H, Jin Y, Ren G. Interpretable Prediction of Pedestrian Crossing Intention: Fusion of Human Skeletal Information in Natural Driving Scenarios. *IEEE Transactions on Intelligent Transportation Systems*, 2024, 25(11): 18153–18170. https://doi.org/10.1109/tits.2024.3435991.

[7] Wang TW, Lai SH. Multi-Modal Pedestrian Crossing Intention Prediction with Transformer-Based Model. *APSIPA Transactions on Signal and Information Processing*, 2024, 13(5). https://doi.org/10.1561/116.20240019.

[8] Xu L, You S, He G, *et al.*. Pedestrian-Vehicle Information Modulation for Pedestrian Crossing Intention Prediction. *IEEE Transactions on Intelligent Vehicles*, 2025, 10(3): 1919–1930. https://doi.org/10.1109/tiv.2024.3437779.

[9] Yang B, Zhu J, Hu C, *et al.*. Faster Pedestrian Crossing Intention Prediction Based on Efficient Fusion of Diverse Intention Influencing Factors. *IEEE Transactions on Transportation Electrification*, 2024, 10(4): 9071–9087. https://doi.org/10.1109/tte.2024.3360966.

[10] Liu H, Liu C, Chang F, *et al.*. Long–Short Observation-driven Prediction Network for pedestrian crossing intention prediction with momentary observation. *Neurocomputing*, 2025, 614: 128824. https://doi.org/10.1016/j.neucom.2024.128824.

[11] Chen X, Xu W, Zhang S, *et al.*. Pedestrian Crossing Intention Prediction via Progressive Multimodal Token Fusion for Autonomous Driving. *IEEE Transactions on Intelligent Transportation Systems*, 2025, 26(9): 12959–12973. https://doi.org/10.1109/tits.2025.3567892.

[12] Chen X, Zhang S, Xu W, *et al.*. Robust Pedestrian Crossing Intention Prediction via Uncertainty-Guided Transformer Ensemble Network for Autonomous Driving. *IEEE Transactions on Instrumentation and Measurement*, 2025, 74: 1–13. https://doi.org/10.1109/tim.2025.3575998.

[13] Chen H, Sun J, Liu Y, *et al.*. Causal Confusion in Pedestrian Crossing Intention Prediction for Autonomous Vehicles: The Role of Ego-Vehicle Speed. *IEEE Transactions on Intelligent Transportation Systems*, 2025, 26(8): 12224–12237. https://doi.org/10.1109/tits.2025.3557125.

[14] Zou H, Guo Y, Wei F, *et al.*. A pedestrian group crossing intention prediction model integrating spatiotemporal features. *Scientific Reports*, 2025, 15(1): 20675. https://doi.org/10.1038/s41598-025-05128-4.

[15] Gazzeh S, Presti LL, Douik A, *et al.*. Context-ped: multi-modal context fusion for pedestrian crossing intention prediction. *Machine Vision and Applications*, 2025, 36(6): 132. https://doi.org/10.1007/s00138-025-01751-3.

[16] Shen X, Raksincharoensak P. Pedestrian-Aware Statistical Risk Assessment. *IEEE Transactions on Intelligent Transportation Systems*, 2022, 23(7): 7910–7918. https://doi.org/10.1109/tits.2021.3074522.

[17] Zhou S, Xu H, Zhang G, *et al.*. Deep learning-based pedestrian trajectory prediction and risk assessment at signalized intersections using trajectory data captured through roadside LiDAR. *Journal of Intelligent Transportation Systems*, 2024, 28(6): 793–805. https://doi.org/10.1080/15472450.2023.2209912.

[18] Schuetz E, Flohr FB. A Review of Trajectory Prediction Methods for the Vulnerable Road User. *Robotics*, 2023, 13(1): 1. https://doi.org/10.3390/robotics13010001.

[19] Sighencea BI, Stanciu RI, Căleanu CTLD. A Review of Deep Learning-Based Methods for Pedestrian Trajectory Prediction. *Sensors*, 2021, 21(22): 7543. https://doi.org/10.3390/s21227543.

[20] Chen K, Song X, Ren X. Modeling social interaction and intention for pedestrian trajectory prediction. *Physica A: Statistical Mechanics and its Applications*, 2021, 570: 125790. https://doi.org/10.1016/j.physa.2021.125790.

[21] Chen CH. A Hybrid Multi-Criteria Decision-Making Approach Based on ANP-Entropy TOPSIS for Building Materials Supplier Selection. *Entropy*, 2021, 23(12): 1597. https://doi.org/10.3390/e23121597.

[22] Lamrini L, Abounaima MC, Alaoui MT. New distributed-topsis approach for multi-criteria decision-making problems in a big data context. *Journal of Big Data*, 2023, 10(1): 97. https://doi.org/10.1186/s40537-023-00788-3.

[23] Storey VC, Hevner AR, Yoon VY. The design of human-artificial intelligence systems in decision sciences: A look back and directions forward. *Decision Support Systems*, 2024, 182: 114230. https://doi.org/10.1016/j.dss.2024.114230.

[24] Meyer J. Doing artificial intelligence (AI): Algorithmic decision support as a human activity.. *Decision*, 2024, 11(4): 481–492. https://doi.org/10.1037/dec0000241.